THE JOURNAL OF BIOLOGICAL CHEMISTRY VOL. 286, NO. 49, pp. 42545–42554, December 9, 2011

An Environment-dependent Structural Switch Underlies the Regulation of Carnitine Palmitoyltransferase 1A*[S]◆

Received for publication, September 22, 2011 Published, JBC Papers in Press, October 11, 2011, DOI 10.1074/jbc.M111.306951

Jampani N. Rao[‡1], Gemma Z. L. Warren[§2], Sara Estolt-Povedano[§], Victor A. Zammit[§2], and Tobias S. Ulmer[‡3]

From the [‡]Department of Biochemistry and Molecular Biology and Zilkha Neurogenetic Institute, Keck School of Medicine, University of Southern California, Los Angeles, California 90033 and the [§]Metabolic and Vascular Health Division, Warwick Medical School, University of Warwick, Gibbet Hill Road, Coventry, CV4 7AL, United Kingdom

Background: The enzyme carnitine palmitoyltransferase 1 regulates the rate of fatty acid oxidation.
Results: The regulatory domain of the enzyme constitutes an amphiphilic structural switch.
Conclusion: The switch can integrate enzyme inhibitor concentration and membrane characteristics into one regulatory signal.
Significance: This represents a highly sophisticated regulatory mechanism for enzymes residing at the membrane-water interface.

The enzyme carnitine palmitoyltransferase 1 (CPT1), which is anchored in the outer mitochondrial membrane (OMM), controls the rate-limiting step in fatty acid β-oxidation in mammalian tissues. It is inhibited by malonyl-CoA, the first intermediate of fatty acid synthesis, and it responds to OMM curvature and lipid characteristics, which reflect long term nutrient/hormone availability. Here, we show that the N-terminal regulatory domain (N) of CPT1A can adopt two complex amphiphilic structural states, termed Nα and Nβ, that interchange in a switch-like manner in response to offered binding surface curvature. Structure-based site-directed mutageneses of native CPT1A suggest Nα to be inhibitory and Nβ to be noninhibitory, with the relative Nα/Nβ ratio setting the prevalent malonyl-CoA sensitivity of the enzyme. Based on the amphiphilic nature of N and molecular modeling, we propose malonyl-CoA sensitivity to be coupled to the properties of the OMM by Nα-OMM associations that alter the Nα/Nβ ratio. For enzymes residing at the membrane-water interface, this constitutes an integrative regulatory mechanism of exceptional sophistication.

Mitochondrial oxidative phosphorylation is the primary source of ATP formation in eukaryotes. In most mammalian tissues, this process utilizes either pyruvate or long chain fatty acids (LCFA)[4] as substrates. Carnitine palmitoyltransferase 1 (CPT1), which is an integral protein of the outer mitochondrial membrane (OMM), converts LCFA-CoA esters to carnitine esters. This permits access of the acyl moieties into the mitochondrial matrix, where CPT2 mediates their conversion back to CoA esters followed by their β-oxidation (1, 2). The inhibition of CPT1 by malonyl-CoA (MCoA), the first intermediate of fatty acid synthesis, enables the enzyme to exert major control over the rate of fatty acid oxidation in all tissues. MCoA acts as a stringent physiological inhibitor of the liver and heart/muscle isoforms CPT1A and -B, respectively (3, 4). Moreover, the sensitivity of CPT1A to MCoA inhibition is markedly affected by the lipid composition and fluidity of the OMM, both when they change physiologically, for example under starvation or diabetes (5, 6) or when the fluidity of the membrane is altered experimentally *in vitro* (7). This correlation to the longer term physiological state endows CPT1A with a pivotal metabolic role in fuel selection, particularly in pathological conditions such as type 2 diabetes and obesity (8, 9) for the treatment of which CPT1A is a drug target (10). In addition, CPT1A shows very different enzyme kinetics depending whether it resides within the bulk outer membrane or in the contact sites that exist between this membrane and the inner membrane of mitochondria (11).

CPT1A consists of a short, well conserved N-terminal regulatory domain (N) and a large C terminal catalytic domain (CD), which are linked by two transmembrane segments that span the OMM (Fig. 1, *A* and *C*). As demonstrated by cross-linking experiments (6), complementary mutagenesis (12), and protein engineering (13), MCoA sensitivity is modulated by a poorly understood interaction between N and CD. Specifically, mutagenesis studies have identified two classes of mutations within N (12, 14–16). Substitutions or deletions involving approximately the first 18 residues decrease MCoA sensitivity, whereas substitutions or deletions within residues 19–40 increase MCoA sensitivity (16). The ability to increase MCoA sensitivity is noteworthy because essentially random mutations

* This work was supported, in whole or in part, by National Institutes of Health Grant HL089726 (to T. S. U.). This work was also supported by The John Douglas French Alzheimer's Foundation.
◆ This article was selected as a Paper of the Week.
[S] The on-line version of this article (available at http://www.jbc.org) contains supplemental Table S1 and Figs. S1–S4.
The atomic coordinates and structure factors (code 2le3) have been deposited in the Protein Data Bank, Research Collaboratory for Structural Bioinformatics, Rutgers University, New Brunswick, NJ (http://www.rcsb.org/).
[1] Present address: Dept. of Physiology, University of Pennsylvania, 3700 Hamilton Walk, A501 Richards Bldg., Philadelphia, PA 19104.
[2] Supported by the British Heart Foundation.
[3] Supported by the University of Southern California Liver Center. To whom correspondence should be addressed: 1501 San Pablo St., ZNI 111, Los Angeles, CA 90033. Tel.: 323-442-4326; Fax: 323-442-4404; E-mail: tulmer@usc.edu.
[4] The abbreviations used are: LCFA, long chain fatty acid; OMM, outer mitochondrial membrane; DDMG, zwitterionic *n*-decyl-*N*,*N*-dimethylglycine; HDAC, hexadecyltrimethylammonium chloride; MCoA, malonyl-CoA; N, N-terminal regulatory domain; OM, *n*-octyl-β-D-maltopyranoside; TDAC, tetradecyltrimethylammonium chloride; DAC, decyltrimethylammonium chloride; DDAC, dodecyltrimethylammonium chloride; PCoA, palmitoyl-CoA; PDB, Protein Data Bank.

are unlikely to increase the affinity between N and MCoA or CD, pointing to the evolution of an intricate regulatory mechanism at the membrane-water interface. Also noteworthy are the common structural features of the MCoA inhibitor and PCoA substrate (Fig. 1*B*), which raises the question as to how the enzyme differentiates between both compounds in the context of N-CD interactions when only the CoA moiety protrudes from the active site (Fig. 1*A*).

Although it is possible to express full-length CPT1A heterologously in *Pichia pastoris* (17), structural studies of CPT1 that could provide a rationale for its complex regulatory mechanism have not been achieved yet perhaps because of its membrane association. However, the catalytic domain of CPT1A shares an ~30% sequence identity with other MCoA-insensitive acyltransferases of known structure, including carnitine acetyltransferase, choline acetyltransferase, and CPT2 (18–21). This level of sequence homology permits the construction of meaningful CD structural models (*e.g.* Fig. 1*A*), which can explain the effects of certain point mutations within the CD (22–24). To provide structural insight into the CPT1 regulatory mechanism, it therefore appears most relevant to characterize the structure of the N-terminal domain. A structural model for N has been discussed (12), but without significant sequence identity to known structures, modeling appears challenging in this case. In addition, the absence of an explanation as to how CPT1A senses the molecular properties of the membrane and integrates them into the MCoA concentration-dependent signal warrants structural studies of N in the presence of membrane mimics.

Here, we used multidimensional, heteronuclear NMR spectroscopy to reveal two alternative structures for the N-terminal regulatory domain of CPT1A. Structure-based site-directed mutageneses in conjunction with functional assays of the full-length protein ascribe physiological relevance to both structures and suggest that their environment-dependent population ratio is used to integrate MCoA concentration, membrane composition, and curvature into one regulatory signal. In combination with molecular modeling of the N·MCoA·CD complex, the structural basis of CPT1A regulation is proposed. These results provide fundamental insight into the regulation of enzymes residing at the membrane-water interface.

EXPERIMENTAL PROCEDURES

Expression and Purification of N-terminal CPT1A Peptide—Using the cDNA of human liver carnitine palmitoyltransferase 1 (CPT1A), isoform 2 (Mammalian Gene Collection Image 3352642; UniProtKB entry P50416) as template, an insert encompassing Met^1–Lys^{42} was generated by PCR and subcloned into the pET-44 expression vector (Novagen, Inc.) with the third IgG-binding domain of protein G (GB3) as N-terminal fusion protein and an intervening tobacco etch virus protease cleavage site. A truncation variant, N(ΔMet^1–Val^8), and G18A point mutation were subsequently constructed using standard techniques.

Expression was induced in *Escherichia coli* BL21-(DE3)pLysS,$T1^R$ cells (Sigma) cultured at 37 °C in M9 minimal medium, containing combinations of 99% ^{13}C-labeled D-glucose, 99% $^{15}NH_4Cl$, and 99% D_2O, at an A_{600} of 1.0 by adding isopropyl 1-thio-β-D-galactopyranoside to 1.0 mM. Cells were lysed by sonication in 50 mM NaH_2PO_4/Na_2HPO_4, pH 7.4, 300 mM NaCl, 100 mM SDS, 20 mM imidazole, 2 mM β-mercaptoethanol. The clarified lysate was applied on a HiTrap IMAC HP column (GE Healthcare) charged with Ni^{2+} for immobilized metal affinity chromatography. The column was washed with 50 mM NaH_2PO_4/Na_2HPO_4, pH 7.4, 300 mM NaCl, 25 mM SDS, and bound protein was eluted in 50 mM Tris·HCl, pH 8.0, 300 mM NaCl, 8 M urea, 300 mM imidazole. The N peptide was cleaved from the fusion protein using tobacco etch virus protease at a molar ratio of 1:50 overnight at 30 °C in 50 mM Tris·HCl, pH 8.0, 0.5 mM EDTA, 1 mM DTT, 100 mM NaCl solution, leaving Met^1 as the N-terminal residue (25). Uncleaved protein and fusion protein were removed by immobilized metal affinity chromatography, and the column flow-through was applied on a Hamilton PRP-3 reverse-phase HPLC column. N peptide was eluted using a linear gradient from 70:30% buffer A (H_2O, 0.1% TFA)/buffer B (80% acetonitrile, 0.1% TFA) to 25:75% in 40 min. Peptide purity was verified by SDS-PAGE and NMR subsequent to freeze-drying.

NMR Sample Preparation—N peptide concentration was measured in acetonitrile/water solution by UV spectroscopy ($\epsilon_{280\ nm}$ = 6,990 M^{-1} cm^{-1}), and defined amounts of peptide were freeze-dried. Peptide was taken up in a volume of 280 μl to yield the following solutions: 0.5 mM N, 25 mM MES·NaOH, pH 5.6, 150 mM DAC; 0.5 mM N, MES·NaOH, pH 5.6, 150 mM DDAC; 0.25 mM N, 25 mM HEPES·NaOH, pH 7.4, 100 mM TDAC; 0.25 mM N, 25 mM HEPES·NaOH, pH 7.4, 100 mM HDAC; 0.5 mM N, 25 mM HEPES·NaOH, pH 7.4, 250 mM OM; and 0.25 mM N, 25 mM HEPES·NaOH, pH 7.4, 200 mM DDMG. The N peptide·DDAC micelle complex was aligned relative to the magnetic field by stretched, negatively charged polyacrylamide gel of 320-μl volume, which was polymerized from a 4.6% w/v solution of acrylamide, 2-acrylamido-2-methyl-1-propanesulfonate, and bisacrylamide with a monomer-to-cross-linker ratio of 39:1 (w/w) and a molar ratio of 98:2 of acrylamide to 2-acrylamido-2-methyl-1-propanesulfonate (26). Upon transferring the gel into an open-ended NMR tube, a ^2H splitting of 2.1 Hz was observed following overnight equilibration.

NMR Spectroscopy—NMR experiments were carried out on a cryoprobe-equipped Bruker Avance 700 spectrometer at 35 °C. Data were processed and analyzed with the nmrPipe package and CARA. $^2H/^{13}C/^{15}N$-labeled N peptide and TROSY-type H-N detection (27) were used for HNCA-, HNCACB-, and HNCO-based backbone assignments, the measurement of $^3J_{C'C\gamma}$ and $^3J_{NC\gamma}$ couplings (28), and the detection of $^1J_{NH}$, $^1J_{C\alpha C'}$, and $^1J_{C'N}$, as well as $^1J_{NH} + {}^1D_{NH}$, $^1J_{C\alpha C'} + {}^1D_{C\alpha C'}$, and $^1J_{C'N} + {}^1D_{C'N}$ couplings (29–31) using isotropic and aligned samples, respectively. $\{^1H\}$-^{15}N NOE measurements were carried out also using deuterated peptide with 5 s of presaturation preceded by a recycling delay of 4 s for the NOE experiment and a 9-s recycle delay for the reference experiment. Aliphatic side chain assignments of a protonated sample were achieved using HAHB(CBCACO)NH, (H)CCC(CO)NH, and H(C)CC-(CO)NH experiments (32). Interproton NOEs were measured by ^{15}N-edited NOESY and HSQC-NOESY-TROSY experiments (120-ms mixing time) in H_2O using protonated and deu-

terated peptide, respectively. A ^{13}C-edited NOESY spectrum, optimized for the detection of aliphatic nuclei, was recorded with a mixing time of 120 ms in D_2O solution.

Structure Calculations—The DDAC-bound N peptide structure of the well folded Ala^{9}–Trp^{39} residues (Fig. 3*B*) was calculated by simulated annealing, starting at 3000 K using the program XPLOR-NIH (33). The peptide termini were represented by random-coil conformations. Except for Gly^{18}, ϕ, θ backbone dihedral angle constraints were derived from N, H^{α} C^{α}, C^{β}, and C′ chemical shifts using the program TALOS+ (34). χ_1 side chain angle restraints were derived from the $^{3}J_{C'C\gamma}$ and $^{3}J_{NC\gamma}$ coupling constants (supplemental Table S1). NOE interproton distance restraints were referenced to the linear α-helical structure of His^{25}–Trp^{39}. In addition to standard force field terms for covalent geometry (bonds, angles, and improper dihedrals) and nonbonded contacts (van der Waals repulsion), dihedral angle and interproton distance restraints were implemented using quadratic square well potentials, and a backbone-backbone hydrogen-bonding potential and torsion angle potential of mean force were employed (35, 36). The difference between predicted and experimental residual dipolar couplings ($\Delta^{1}D$) was described by a quadratic harmonic potential. The final values for the force constants of the different terms in the simulated annealing target function are as follows: 1,000 kcal·mol^{-1}·Å^{-2} for bond lengths; 500 kcal·mol^{-1}·rad^{-2} for angles and improper dihedrals, which serve to maintain planarity and chirality; 4 kcal·mol^{-1}·Å^{-4} for the quartic van der Waals repulsion term; 30 kcal·mol^{-1}·Å^{-2} for interproton distance restraints; 500 kcal·mol^{-1}·rad^{-2} for dihedral angle restraints; 0.3 kcal·mol^{-1}·Hz^{-2} for $^{1}D_{NH}$ residual dipolar couplings restraints, and $^{1}D_{C'N}$ and $^{1}D_{C\alpha C'}$ scaled relative to $^{1}D_{NH}$ according to their dipolar interaction constants; 1.0 for the torsion angle potential; and a directional force of 0.20 and a linearity force of 0.05 for the hydrogen-bonding potential. A total of 20 structures were calculated (Table 1). Coordinates, chemical shifts, and structural constraints for Nβ have been deposited in the Protein Data Bank as code 2le3 and BMRB with accession number 17690.

CPT1A Homology Modeling and N Docking—An atomic resolution model of the CD of human CPT1A (residues 168–766) was derived from rat choline acetyltransferase (PDB code 1T1U; 29% sequence identity) by homology modeling (37). Similar results were obtained when using mouse carnitine acetyltransferase (PDB code 1NDB) or rat choline acetyltransferase (PDB code 1Q6X) templates. Docking calculations with Nβ were performed using the program ClusPro 2.0 (38). MCoA was placed in the CoA and carnitine binding pockets of the Nβ·CD models using the complexes of the CD of mouse carnitine acetyltransferase with CoA and carnitine, respectively (PDB codes 1ndi and 1ndf, respectively) (20), as templates.

Assay of CPT1 Activity—The construction of the pGAPZ plasmid expressing wild type rat CPT1A has been described previously (16). The point mutations in CPT1A (Fig. 6) were prepared by QuikChange PCR. Transformation into and expression in *P. pastoris* strain X-33 were performed according to the expression system distributor Invitrogen. Mitochondrially enriched cell-free extracts from *P. pastoris* expressing CPT1A were prepared and assayed for CPT activity with L-[*N-methyl*-^{3}H]carnitine hydrochloride as described previously (17). Briefly, the standard assay buffer contained 150 mM KCl, 1 mM EGTA, 20 mM HEPES, pH 7.2, 1% (w/v) fatty acid-free BSA, and 1 mM dithiothreitol. Reactions were prepared in duplicate with palmitoyl-CoA added to a final concentration of 35 μM and the addition of varying amounts of malonyl-CoA in a final volume of 1.1 ml. Yeast extract was added, and reactions were heated to 30 °C for 2 min before the addition of L-[^{3}H]carnitine to a final concentration of 500 μM and then incubated for a further 4 min before termination of the reaction by addition of 0.3 ml of 6 M HCl and transfer to ice. [^{3}H]Palmitoylcarnitine was extracted into butan-1-ol at low pH and determined by liquid scintillation counting. Nonlinear curve fitting and calculation of enzyme kinetic parameters were performed as described previously (16, 39). Intrinsic enzyme activities were unchanged relative to the wild type when normalized for the level of protein expression as quantified on Western blots by anti-C antibodies (40).

RESULTS AND DISCUSSION

N-terminal CPT1A Domain Can Adopt Two Structural States—Based on the functional properties of CPT1, we hypothesized that N might associate with the CD, with the OMM or exist "free" within the aqueous environment (Fig. 1*A*). To address this hypothesis, a peptide, also termed N, corresponding to the first 42 residues of human CPT1A (Fig. 1*C*) was prepared recombinantly. N was found to be insoluble in aqueous solution, suggesting that, in native CPT1A, it cannot exist free in the cytosol. If N were to associate with the OMM, an amphiphilic structure would be required. To detect and stabilize such a structure, we investigated its interaction with phospholipid bicelles and detergent micelles, which constitute well established model systems for the study of protein-membrane interactions (41, 42). Upon screening an extensive array of different bicelles and micelles, N was found to be amenable to structural characterization by NMR spectroscopy in the presence of several micelle systems (Fig. 2*A*).

Depending on the micelle system employed, one of two characteristic H^{N}-N peak patterns was observed (Fig. 2, *B* and *C*). One of these states, termed Nα, was observed in the presence of cationic tetra- or hexadecyltrimethylammonium chloride (TDAC or HDAC) micelles (Fig. 2, *A* and *B*). The second state, termed Nβ, was obtained not only in the presence of neutral *n*-octyl-β-D-maltopyranoside (OM) and zwitterionic DDMG micelles but, unexpectedly, also in the presence of decyl- and dodecyltrimethylammonium chloride (DAC and DDAC) micelles (Fig. 2, *A* and *C*). DDAC and TDAC differ in the length of their hydrocarbon tails by two methylene groups (Fig. 2*A*), giving rise to different micelle sizes. Like DAC and DDAC, OM and DDMG also exhibit relatively short hydrocarbon tails (Fig. 2*A*), which are anticipated to result in small micelles (low aggregation numbers). Thus, among the detergents studied, micelle size rather than headgroup identity determined the structural state of N. This invariance to a wide range of headgroup types clearly indicates that micelles are suitable membrane mimics for N.

To examine the influence of the micelle system on Nα and Nβ formation in more detail, $^{13}C^{\alpha}$ chemical shift assignments

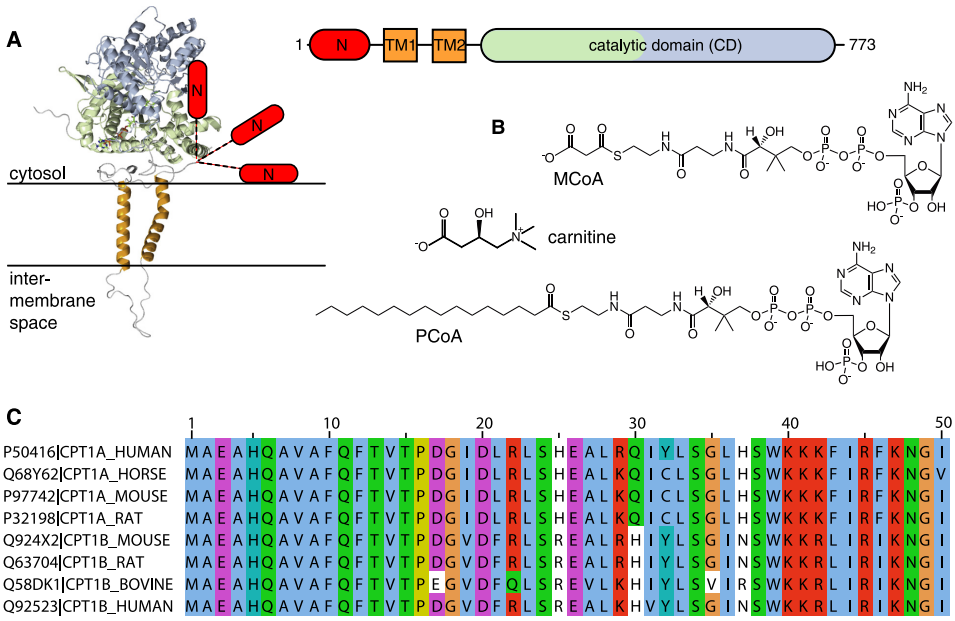

FIGURE 1. **Overview of CPT1A system.** *A*, domain organization and homology model of the CPT1A structure without the N-terminal regulatory element (*N*) for which no homologous structure exists. Possible N association states (OMM-associated, free in cytosol, and CD-associated) are shown schematically. Bound MCoA is illustrated in *ball-and-stick* representation. The CPT1A membrane topology is known (60), but the relative orientations of the transmembrane (*TM*) and CD domains are unknown, and depicted is one possible arrangement. *B*, chemical structures of physiological enzyme inhibitor (MCoA) and substrates (palmitoyl-CoA (*PCoA*) and carnitine). The common CoA moiety of inhibitor and substrate is noted. *C*, sequence alignment of N of CPT1A and -1B. Conserved amino acids are colored by the Jalview multiple alignment editor (61) using the ClustalX color scheme.

were performed for N bound to OM and the four trimethylammonium-based micelles studied (Fig. 2*A*). With increasing tail lengths, these latter micelles exhibit aggregation numbers of 30, 44, 62, and 84, respectively (43, 44), and thus offer a continuous increase in micelle surface area paired with a decrease in scaffold curvature. In contrast to $^{1}H^{N}$-^{15}N chemical shifts, $^{13}C^{\alpha}$ chemical shifts correlate directly with backbone torsion angles (45, 46), rendering them powerful probes of protein conformation. For the five micelle systems studied, only two sets of $^{13}C^{\alpha}$ chemical shifts were observed (Fig. 3*A*). Consequently, N exhibited virtually identical backbone conformations when bound to OM, DAC, or DDAC micelles, as well as when associated with TDAC or HDAC micelles. This observation demonstrated that the conformation of N does not change gradually and continuously according to the size of the micelles provided but interconverts between Nα and Nβ in a switch-like manner when a discrete micellar size threshold is reached.

In conclusion, micellar membrane mimics support an association of N with the OMM. Because there are two functionally opposing types of mutations within the N-terminal domain of CPT1A with respect to the effects on MCoA sensitivity (12, 14–16), the detection of two structural states may be significant. N is relatively small (Fig. 1, *A* and *C*) and an amphiphilic association with the OMM may require the N-CD association to be also of amphiphilic nature, *i.e.* micelles may act as folding scaffolds for the OMM- as well as the CD-associated state of the N-terminal regulatory domain.

Structure of Nβ State—To elucidate the structural basis of the switch-like behavior of N and to assign functionality to the respective structural states, the structure of Nβ was determined by multidimensional, heteronuclear NMR spectroscopy. Simulated annealing calculations based on residual dipolar coupling, close interproton distance, and backbone and side chain torsion angle restraints were carried out, resulting in an ensemble of a total of 20 structures for which a coordinate precision of 1.03 Å was obtained for heavy atoms (Fig. 4*A*). A summary of structural statistics is provided in Table 1. Despite the relatively small size of N, a complex structure, encompassing α-helix, β-sheet, β-turn, as well as an unstructured stretch, was found (Fig. 4, *A* and *B*). The eight N-terminal residues of Nβ (Met^{1}–Val^{8}) were unstructured and were followed by an anti-parallel β-sheet, comprising sheets β1 (Phe^{10}–Val^{14}) and β2 (Ile^{19}–Leu^{23}). At the C terminal end of the peptide, an α-helix, termed α2, was present encompassing His^{25}–Trp^{39} (Fig. 4*A*). The β1-β2 connection was formed by Thr-Pro-Asp-Gly, constituting a hairpin of canonical sequence (47). Ser^{24} mediated the transition between β2 and α2. It entertained backbone-to-backbone hydrogen bonds with both the C=O of the first structured residue (Ala^{9}) and the N-H group of Leu^{28}. Moreover, close contacts between Ser^{24}(O^{γ}) and Glu^{26}(H^{N}) as well as Ala^{27}(H^{N}) were detected, providing further capping of helix α2 (Fig. 4*C*). Another notable feature of Nβ was the hydrophobic packing interaction between the methyl groups of Ala^{27} and Ala^{9} (Fig. 4*C*). With the exception of Phe^{12} and Tyr^{32}, side chain rotamers were averaged (supplemental Table S1). The regular secondary structure elements of Nβ showed backbone dynamics characteristic of well ordered structural elements as evidenced by close to maximal {^{1}H}-^{15}N NOE values (Fig. 3*B*). Slight decreases in backbone dynamics were noticeable between secondary structure transitions (Thr^{15}–Gly^{18} and Ser^{24}).

The Nβ structure was found to be distinctly amphiphilic, which would have been difficult to predict from its primary sequence (Fig. 1*C*). The residues lining each side of the β1-β2

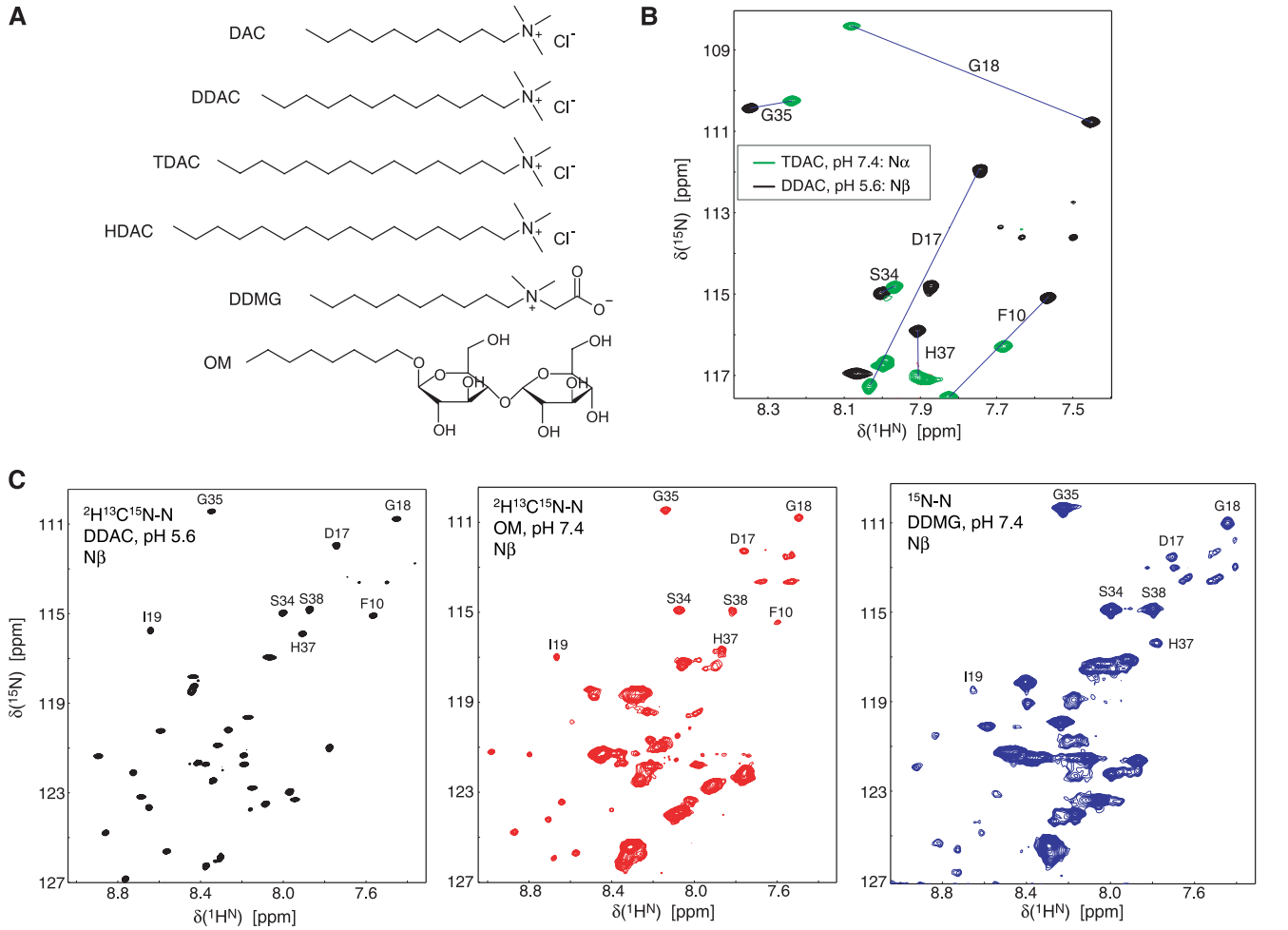

FIGURE 2. **Comparison of employed micelles systems and ensuing NMR spectra.** *A*, chemical structures of successfully employed detergents DAC, DDAC, TDAC, and HDAC, as well as OM and zwitterionic DDMG. *B*, representative section of $^{1}H^{N}$-^{15}N correlation spectra of N bound to DDAC and TDAC micelles, resulting in Nα and Nβ states, respectively. *C*, $^{1}H^{N}$-^{15}N correlation spectra of Nβ bound to the micelles indicated. Selected backbone assignments are shown. All spectra were recorded at 35 °C and a ^{1}H frequency of 700 MHz.

interface are either hydrophobic or charged/polar, and helix α2 exhibits distinctly amphiphilic periodicity (Fig. 4, *B* and *D*). N therefore exhibits tertiary amphiphilicity, which is rare (48). Between the longitudinal axes of β1-β2 and α2, an angle of ~105° was obtained, providing a rationalization for the preference of Nβ to associate with relatively small, highly curved micelle scaffolds. The nonplanar structure of Nβ makes it suitable to associate with the CD (Fig. 1*A*).

Description of Nα State and Nα ↔ Nβ Switching Determinant—From the difference of $^{13}C^{\alpha}$ chemical shifts of Nα and Nβ (Fig. 3*A*), it was evident that both states share helix α2 but diverge otherwise. Specifically, for Nα, the structure comprising sheets β1-β2 became destabilized concomitant to the establishment of an N-terminal helix comprising Ala^{2}–Val^{8}, termed α1 (Fig. 3*A*). The stability of α1 was lower than that of α2 (Fig. 3*B*), and therefore, helix α1 must be considered to be only partially folded under the current experimental conditions. However, we note that, due to post-translational processing, CPT1 commences with acetylated Ala^{2} (49), which is an efficient helix-capping motif (50). Under *in vivo* conditions, the helical propensity of Ala^{2}–Ala^{8} in Nα may therefore be promoted further. In the context of only partially ordered α1 and β1-β2 secondary structures, the structural description of Nα must remain illustrative for these regions at present. Fig. 5 depicts a model that was based on the interpretation of chemical shifts (34) and the overall tertiary arrangement of Nβ. Whereas helix α2 is well structured, any global Nα structure merely represents one possible α1/β1-β2 conformation out of an ensemble of partially folded structural states. We propose that the Nα structure, which is formed when the β1-β2 conformation is destabilized, will have a propensity to bind to the planar OMM or, alternatively, to the OMM and CD simultaneously (Fig. 1*A*).

The contrast between the Nα and Nβ structures suggests that the formation of α1 and β1-β2 are mutually exclusive. In the Nβ state, Ala^{9} packs against Ala^{27}, which directs the unfolded Met^{1}–Val^{8} residues away from the micelle surface (Fig. 4, *B* and *C*). Similarly, because of steric clashes, helix α1 cannot be formed without compromising the structural integrity of either α2 or β1-β2 (Fig. 5). The mutual exclusivity of α1 and β1-β2 appears to be an intrinsic design feature of N, contributing to the switch-like structural transition between Nα and Nβ. To understand the conformational properties of α1 in more detail, we next investigated whether residual β1-β2 struc-

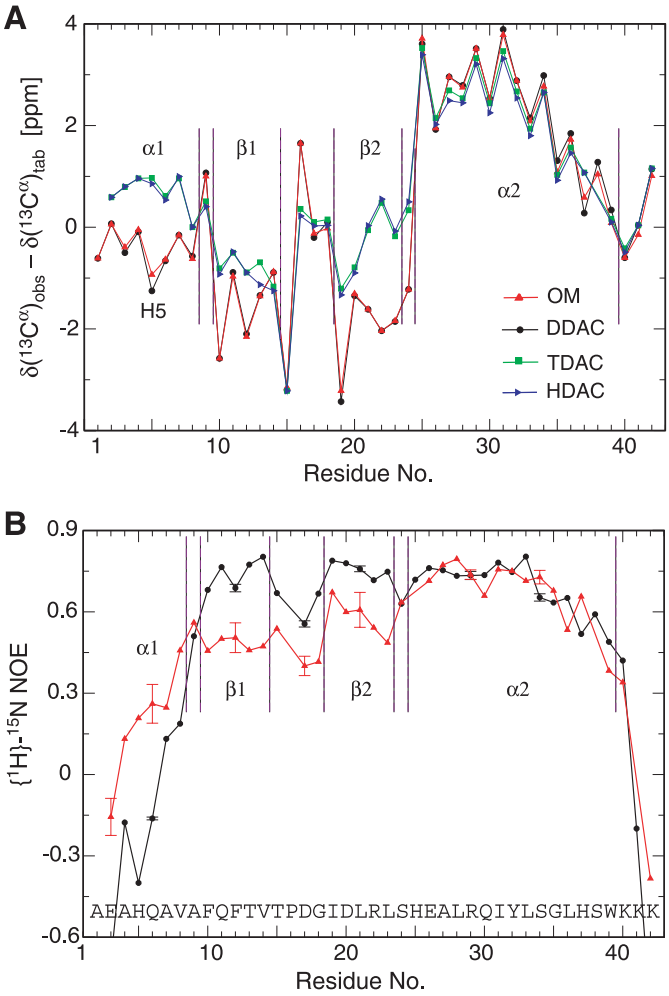

FIGURE 3. **Comparison of structural and dynamic NMR parameter of N bound to different micelles.** *A*, comparison of backbone secondary structure propensities as reflected by secondary $^{13}C^{\alpha}$ chemical shifts. For $^{2}H/^{13}C/^{15}N$-labeled N, random coil conformations are obtained at approximately −0.5 ppm, whereas positive and negative shifts relative to this value denote helical and extended backbone propensities, respectively (45). Shifts for DAC were identical to DDAC and were omitted for the sake of visual clarity. *B*, comparison of backbone order (pico- to nanosecond time scale dynamics) as reflected by {^{1}H}-^{15}N NOE values. Larger values indicate higher order (smaller amplitude H-N amide bond vector dynamics).

tural propensity (Fig. 3) precludes the formation of a stable α1 helix. A G18A substitution in N was generated to abrogate the β-hairpin, as Ala cannot sustain a φ backbone torsion angle range compatible with the hairpin. Compared with the wild type Nβ state, G18A led to a loss of NMR chemical shift dispersion (supplemental Fig. 1*A*), indicating that Nβ could no longer be formed. By contrast, in Nα, the substitution did not increase the helical content of α1, as evidenced by virtually identical $^{13}C^{\alpha}$ chemical shifts between Nα(G18A) and Nα (supplemental Fig. 1*B*). This suggests that, within the context of the micelle system employed, residues Ala^2–Ala^8 had reached their maximum helical content.

The switch from Nβ to Nα was observed upon increasing the micelle size (see above). We tested whether this occurs because of an increase in micelle curvature or an increase in micelle surface area that permitted a greater degree of α1 binding so as to compete with β1-β2 sheet formation. To distinguish between the two possibilities, a peptide lacking the first eight amino acid residues, N(Δ1–8), was studied. This deletion did not rescue Nβ when binding to TDAC micelles (supplemental Fig. 2), showing that curvature *per se* was the sole Nα ↔ Nβ switching determinant and that the micelle systems employed did not restrict the structure adopted by Nα. Therefore, all our data indicate that, as the binding surface curvature is increased, the well defined β1-β2/α2 structure of Nβ cannot be sustained, giving way to the adoption of the α1 helix as the default conformation. The switching curvature threshold would appear to be close to the micelle radius of DDAC of 17.1 Å (43, 44), at which solution conditions can be chosen to obtain Nα and Nβ simultaneously (supplemental Fig. 3). In conclusion, the peptide equivalent to the regulatory domain of CPT1A can undergo an amphiphilic environment-dependent structural switch in which a disturbance in target Nβ binding surface curvature flips Nβ to the default Nα state.

MCoA-dependent Regulation of CPT1A—To assess the functional significance of Nα and Nβ within the native CPT1A environment, we characterized enzyme kinetics, most notably the concentration of MCoA at which half-maximal inhibition (IC_{50} value) is observed, as a function of structure-based point mutations. Following well established protocols (16, 17), rat CPT1A mutants were expressed in the yeast *P. pastoris* where the enzyme resides in its native eukaryotic OMM lipid environment. The N-terminal regulatory domain is fully conserved between human and rat CPT1A except for Y32C (Fig. 1*C*). First, we studied point mutations aimed at modifying key determinants of the Nβ → Nα transition without affecting side chain contacts external to N to avoid altering any N-CD interactions. The G18A and A9G substitutions fall in this category and were predicted to favor the Nβ → Nα transition (Fig. 4 and supplemental Fig. S1). When incorporated into CPT1A, either mutation led to a significant increase in the MCoA sensitivity of the enzyme (Fig. 6) without any change to the intrinsic activity of the expressed proteins (data not shown). This result identified Nα as the conformation that promotes MCoA inhibition, whereas Nβ represents the noninhibitory state. By contrast, disturbing Nα should make CPT1A less sensitive to MCoA inhibition. Because the N switching machinery resides exclusively within the Nβ structure (Ala^9/Ala^{27}, Thr^{15}–Gly^{18}, and Ser^{24}), the reverse Nα → Nβ switch can only be achieved by disturbing putative side chain contacts of Nα with the MCoA·CD complex. We predicted that altering a key side chain within helix α1 (Fig. 5) would decrease MCoA sensitivity. The charge reversal mutation E3R was employed and resulted in a decrease in enzyme sensitivity to MCoA (Fig. 6), in agreement with our expectation of noninhibitory Nβ benefiting from dysfunctional Nα, *i.e.* an increased likelihood of Nα → Nβ transitions. In conclusion, we propose that an Nβ → Nα structural switch of the here-determined structures underlies the MCoA-dependent inhibition of CPT1A.

In the light of our present observations, it is instructive to revisit the mutagenesis data that have established the existence of positive and negative determinants of MCoA sensitivity in the N-terminal domain of CPT1A. Mutations that make CPT1A more sensitive to MCoA localize within β1-β2 and α2 (14) and are anticipated to destabilize the β1-β2/α2 arrangement of Nβ (*e.g.* S24A) or to diminish Nβ affinity to its target

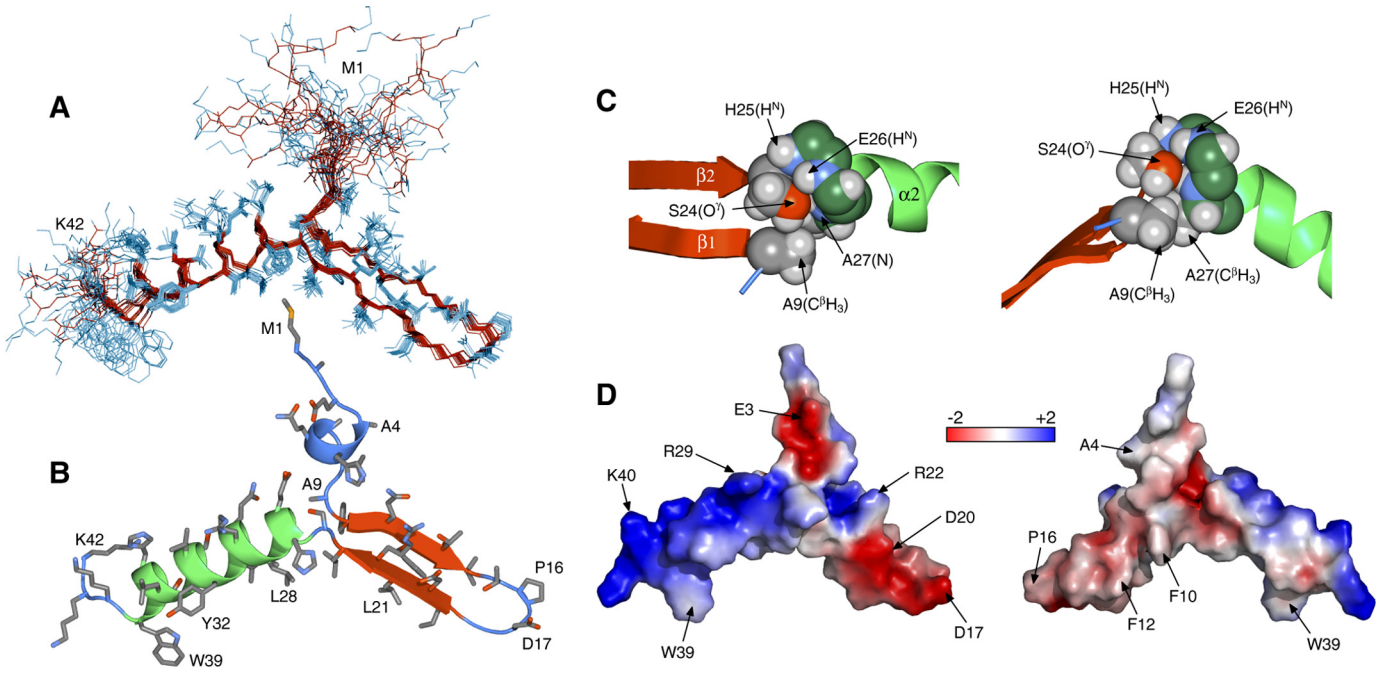

FIGURE 4. **Structure of Nβ (DDAC-bound N at pH 5.6).** *A*, superposition of the ensemble of 20 calculated simulated annealing structures. The peptide termini, Met^1–Val^8 and Lys^{40}–Lys^{42}, were unstructured. *B*, schematic representation of the Nβ structure (lowest energy ensemble member). The helical conformation of Ala^4–Ala^7 was coincidental to this ensemble member only (see *A*). *C*, packing of the β1-β2/α2 transition. The carbon atoms of Ala9 and Ser^{24} are shown in *gray*, and the carbon atom of helix α2 residues His^{25}, Glu^{26}, and Ala^{27} are shown in *dark green*. Oxygen and nitrogen atoms are shown in *red* and *blue*, respectively. *D*, surface charge distribution color-coded by electrostatic potential. The potential was calculated using APBS (62).

TABLE 1

Structural statistics for Nβ (DDAC-bound N peptide)

Statistics for the 20 calculated simulated annealing structures encompassing structured residues Ala^9–$Trp3^9$ are given. Numbers in parentheses indicate number of restraints.

Root mean square deviations from experimental dihedral restraints	
All (75)[a]	0.28 ± 0.04°
Root mean square deviations from experimental residual dipolar couplings (Hz) [b]	
$^1D_{NH}$ (30)	1.55 ± 0.07
$^1D_{NC'}$ (29)	1.97 ± 0.16
$^1D_{C\alpha C'}$ (30)	1.65 ± 0.05
Root mean square deviations from experimental distance restraints	
All (228)	0.05 ± 0.01 Å
Intraresidue (66)	0.03 ± 0.01 Å
Inter-residue sequential ($\|i-j\|=1$) (105)	0.05 ± 0.01 Å
Inter-residue short range ($1<\|i-j\|<5$) (35)	0.07 ± 0.01 Å
Inter-residue long range ($\|i-j\|\geq 5$) (22)	0.06 ± 0.01 Å
Deviations from idealized covalent geometry	
Bonds	0.003 ± 0.000 Å
Angles	0.596 ± 0.016°
Impropers	0.400 ± 0.019°
Coordinate precision[c]	
Backbone non-hydrogen atoms	0.30 Å
All non-hydrogen atoms	1.03 Å
Measures of structural quality	
E_{LJ} (kcal mol^{-1})[d]	−128.9
Residues in most favorable region of Ramachandran plot[e]	99.3%

[a] Torsion angle restraints included 33 φ, 33 ψ, and 9 χ_1 angles.
[b] Root mean square deviations are normalized to an alignment tensor magnitude of 10 Hz.
[c] Date are defined as the average root mean square difference between the final 20 simulated annealing structures and the mean coordinates.
[d] The Lennard-Jones van der Waals energy was calculated with the CHARMM PARAM 19/20 parameters and was not included in the simulated annealing target function.
[e] Data were calculated using PROCHECK version 3.4.4.

surface as a result of losing its amphiphilic nature and/or side chain contacts (*e.g.* G30A and R22A/H25A/K29A). In addition, the Δ(19–30) and Δ(19–46) deletion mutants, which enhance MCoA sensitivity (16), would prevent the β1-β2/α2 arrangement of Nβ altogether (Fig. 4) and may be regarded as achieving a permanent Nβ → Nα switch. By contrast, substitutions or deletions that make CPT1A less sensitive to MCoA localize within helix α1 except for E26K mutations (12, 14–16), which resides in helix α2 and may make contacts with the CD required for inhibition in accordance with the conservation of helix α2 between Nα and Nβ (Figs. 4 and 5). We regard those "negative" mutations as negating the formation of functional Nα by disturbing the formation of key side chain contacts between N and MCoA·CD and/or by interfering with the mildly amphiphilic

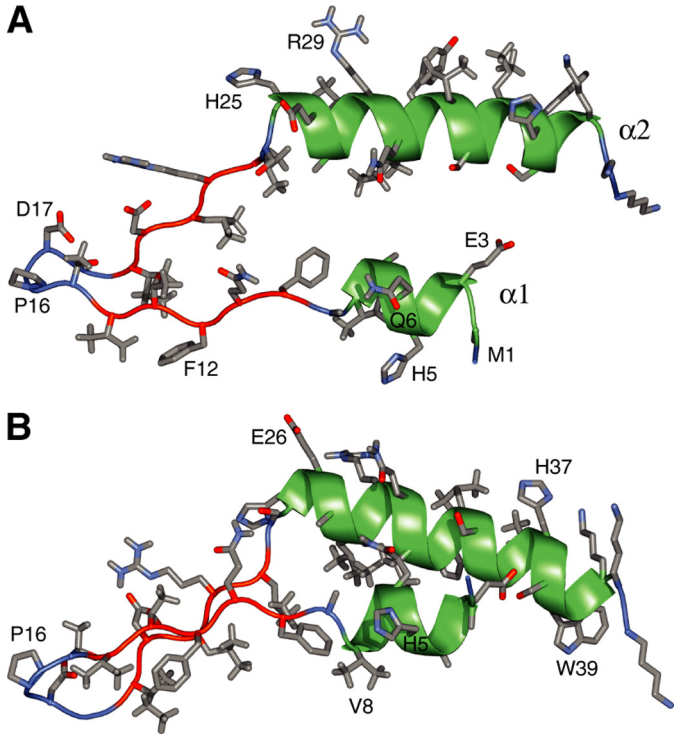

FIGURE 5. **Structural model of Nα (TDAC-bound N at pH 7.4).** *A* and *B*, model illustrates the helical propensity of α1 and stable helix α2. Destabilization of β1/β2 results in the disruption of any defined β-sheet structure. The relative orientations of β1, β2, and α2 are shown in an arrangement similar to Nβ.

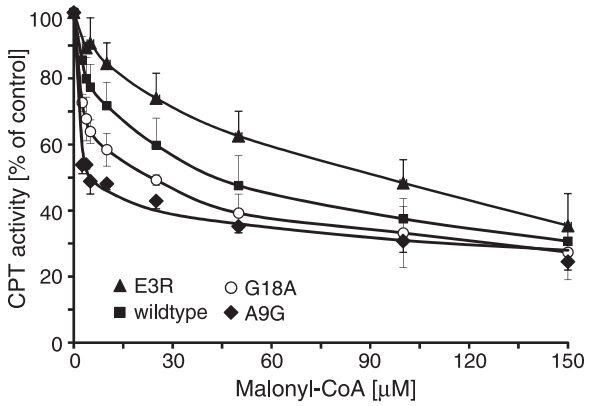

FIGURE 6. **CPT1A structure-based site-directed mutagenesis.** Effects of selected point mutations on the sensitivity of full-length rat CPT1A to MCoA inhibition. Maximal inhibition for each construct was determined to be 80% of control activity. The concentrations of MCoA at which half-maximal inhibition (IC_{50} value) was observed were 56.0 ± 6.8 μM for E3R, 8.1 ± 2.7 μM for G18A, and 1.5 ± 0.3 μM for A9G. The IC_{50} value for the native rCPT1A was 25.0 ± 4.9 μM. Values are means of 3–5 determinations (± S.E.).

nature of α1 (Ala[2], His[5], and Val[8] line the apolar face, and Asp[3], Gln[6], and Ala[7] populate the polar helix face; Fig. 5). In summary, an extensive and consistent body of evidence leads us to propose that the prevalent MCoA sensitivity of CPT1A is determined by the relative population ratio of inhibitory Nα to non-inhibitory Nβ structural states.

OMM-dependent Regulation of CPT1A—The Nα ↔ Nβ switch may also explain the well established dependence of MCoA sensitivity on OMM lipid composition and lipid molecular order/fluidity (5–7). As alluded to earlier, based on the requirement of a strongly curved micelle folding scaffold for the formation of Nβ, this state appears best suited to interact solely with the CD as illustrated in Fig. 7*A*. By contrast, Nα formation requires a less curved surface, and this conformation could be promoted when N is able to bind to the near planar OMM surface or to the OMM and CD simultaneously (Fig. 7*C*). Thus, a high Nα-OMM affinity and, consequently, the facilitation of the Nβ → Nα transition will make CPT1A more prone to inhibition by MCoA. Conversely, in case of a lowered Nα-OMM affinity, the reverse Nα → Nβ transition becomes more probable, thereby decreasing MCoA sensitivity. We therefore propose that the Nα:Nβ balance not only determines the prevalent MCoA sensitivity of CPT1A but simultaneously couples MCoA sensitivity to the properties of the OMM. Structurally, this translates into an inhibitory OMM·Nα·MCoA·CD and a catalytically active Nβ·CD·LCFA-CoA·carnitine complex (Fig. 7, *A* and *C*).

The switch mechanism between the two states of the N-terminal domain of CPT1A provides a regulatory mechanism that enables the enzyme to respond to different metabolic states at multiple levels of organization. Whereas changes in MCoA concentration reflect short term substrate availability and lipogenic enzyme activity, changes in membrane properties derive from the longer term metabolic state (51). This includes changes in lipid composition that occur in response to changes in hormonal balance such as the degree of unsaturation of acyl group composition of phospholipids, the identity of phospholipid headgroup, and the cholesterol/phospholipid ratio of the membrane (5, 51). Finally, we note that contact sites between the outer and inner membrane of mitochondria, which exhibit a high degree of membrane curvature (52, 53), represent an environment where the kinetics of MCoA inhibition with respect to LCFA-CoA shifts from a non-competitive to a competitive mode (11). Membrane curvature in unilamellar vesicles is limited to a radius of ~105 Å (54), whereas Nα ↔ Nβ switching takes place at a radius of ~17 Å (see above). It follows that the high degree of membrane curvature at contact sites may disturb optimal OMM-Nα-MCoA-CD associations (Fig. 7*C*). Therefore, this may represent a further element to the CPT1A regulatory mechanism, as it will make the relative Nα/Nβ ratio also dependent on the degree of membrane curvature of its microenvironment.

Model of the N-CD Interaction—To provide further insight into the structural basis of CPT1A regulation and to illustrate our proposed CPT1A regulatory mechanism, we performed computations that model the docking of Nβ and Nα to a homology model of the CD. Two pertinent Nβ-CD docking results placed Nβ near the carnitine- and CoA-binding site within the CD, respectively (Fig. 7, *A* and *B*). Upon inserting MCoA into the CD structure, according to the mode of CoA binding observed in carnitine acetyltransferase (20), we noted that a displacement of carnitine must take place to accommodate the malonyl carboxylate (Figs. 7*A* and 1*B*). This binding mode is supported by the observation that when the sulfhydryl group of CoA becomes oxidized to sulfonic acid, it occupies the carnitine carboxylate-binding pocket (20). It also explains the competitive relationship between MCoA and carnitine during catalysis, *e.g.* MCoA increases K_m for carnitine (12, 55). It is therefore evident that the binding of MCoA and carnitine/PCoA is structurally distinct at the carnitine-binding pocket. This difference may give rise to an allosteric conformational

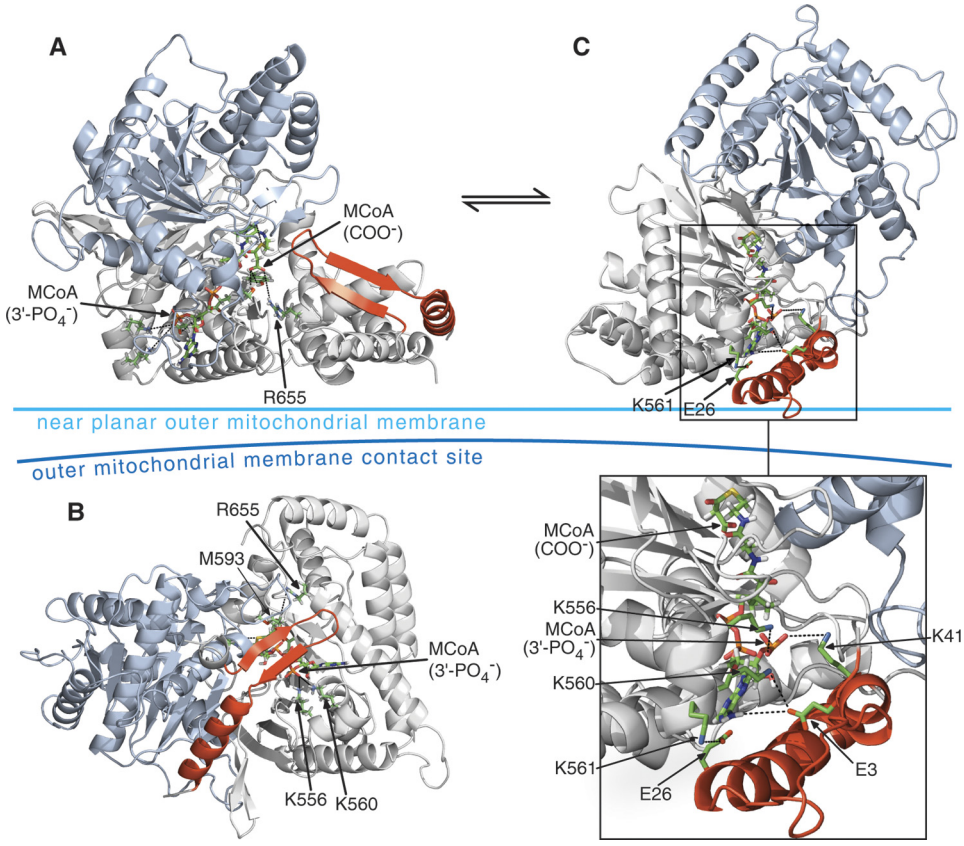

FIGURE 7. **Models of Nβ-CD and Nα-CD associations.** *A* and *B*, models obtained by docking Nβ to a homology model of the CD using the program ClusPro 2.0 (38). *A* places the apex of Nβ over the helix formed by Asp^{654}–Leu^{667}. Arg^{655} of this helix contributes to carnitine binding and is also positioned to interact with MCoA as depicted by *dashed lines*. *B* docks Nβ near the CoA-binding site. This model localizes Nβ closer to CD mutations that affect MCoA sensitivity (*e.g.* Met^{593} (63)), albeit this may merely reflect their proximity to the CoA-binding site to which MCoA can bind as well. *C*, model obtained by manually docking Nα to a homology model of the CD. A Glu^{26}–Lys^{561} salt bridge was enforced. Nα was oriented to permit Glu^{3}–Lys^{560}, Glu^{3}-MCoA(NH_2), and Lys^{41}–MCoA (3′-phosphate) interactions. The outer mitochondrial membrane is expected at the *bottom* of the panel, providing a binding surface for Nα and parts of the CD. Nα is shown in *red*, the N and C domains, making up the catalytic domain (*CD*), are shown in *blue* and *gray*, respectively. Bound MCoA and selected amino acid side chains are illustrated in *ball-and-stick* representation.

change in the CD that increases the Nβ binding surface curvature, thus triggering an Nβ → Nα switch. Binding of Nβ near the carnitine-binding pocket (Fig. 7*A*) may facilitate such a mechanism. Alternative Nβ-CD associations, for example near the CoA-binding site (Fig. 7*B*), are also possible. However, because MCoA inhibitor and PCoA substrate share the CoA moiety and differ chemically only near the active site (Fig. 1*B*), binding of Nβ next to CoA appears to be less suitable to differentiate between inhibitor and substrate binding. An alternative to an allosteric CD conformational change would be a second MCoA-binding site (12) that could also trigger an Nβ → Nα switch if it were to overlap with the Nβ-binding site.

Docking of Nα to the CD domain was complicated by the absence of the OMM in our model but facilitated by a structural constraint derived from complementary mutagenesis. The E26K point mutation decreases MCoA sensitivity of CPT1A, but K561E can compensate for this mutation (12) indicative of the presence of a Glu^{26}–Lys^{561} electrostatic interaction in the Nα·CD complex. In all of our constructed CD models, Lys^{561} pointed away from the enzyme surface and into bulk solvent, disfavoring a docking of Lys^{561} with N embedded in the CD surface. However, in the context of an OMM-bound Nα, such an interaction was readily obtainable (Fig. 7*C*). Because of the lowered dielectric constant of the membrane-water interface compared with bulk water, a membrane-proximal salt bridge would also be stronger than a corresponding solvent-exposed interaction (56). When enforcing an electrostatic Glu^{26}–Lys^{561} interaction in our models, it was found that Nα, and specifically Glu^{3}, has access to positive side chain charges on the CD or to the NH_2 group of the adenosine moiety of CoA (Figs. 7*C* and 1*B*). When evaluated within the context of the micelles used in this study, the NMR spectral properties of both Nα and Nβ were essentially unperturbed by the presence of MCoA (supplemental Fig. 4). However, in the absence of a defined CD-bound MCoA conformation, this result has limited significance. We also note that the commencement of native CPT1A with acetylated Ala^{2} (49) avoids competition for Glu^{3} with an N-terminal positive charge. In summary, a destabilization of the Nβ state effected by MCoA may promote CD inhibition through either OMM-Nα-CD or OMM-Nα-MCoA-CD interactions. Based on our structural OMM·Nα·MCoA·CD model, MCoA-dependent inhibitory actions are explained by a blockage of substrate access to the CD by Nα. In support of this model, kinetics of MCoA inhibition with respect to LCFA-CoA are indeed found to be noncompetitive for the protein within the bulk OMM fraction (11).

Conclusions—The pivotal metabolic role of CPT1A is reflected in the intricate structural properties of its relatively

short N-terminal regulatory domain detected in the presence of micellar folding scaffolds. The properties of N enable an amphiphilic, environment-dependent switch that permits interactions with the CD as well as the OMM. This allows N to integrate information concerning location (membrane curvature), long term metabolic state (membrane fluidity and composition), as well as short term metabolic state (MCoA concentration), providing the structural basis for the molecular "memory" of CPT1A (57). Based on the regulated interconversion of N between different environments, its proposed role is etiologically similar to amphiphilic helices in amphotropic proteins (58). Aside from prominent roles in membrane curvature, sensing, and induction (58, 59), amphiphilic helices can also regulate enzyme activity by responding to ligands or to covalent modifications (58). In comparison, however, the complexity and sophistication of the integrative regulatory mechanism evolved for CPT1A appears unprecedented.

REFERENCES

1. Zammit, V. A., Ramsay, R. R., Bonomini, M., and Arduini, A. (2009) *Adv. Drug Deliv. Rev.* **61,** 1353–1362
2. Akkaoui, M., Cohen, I., Esnous, C., Lenoir, V., Sournac, M., Girard, J., and Prip-Buus, C. (2009) *Biochem. J.* **420,** 429–438
3. McGarry, J. D., Mannaerts, G. P., and Foster, D. W. (1977) *J. Clin. Invest.* **60,** 265–270
4. Saggerson, E. D. (1982) *Biochem. J.* **202,** 397–405
5. Zammit, V. A., Corstorphine, C. G., Kolodziej, M. P., and Fraser, F. (1998) *Lipids* **33,** 371–376
6. Faye, A., Borthwick, K., Esnous, C., Price, N. T., Gobin, S., Jackson, V. N., Zammit, V. A., Girard, J., and Prip-Buus, C. (2005) *Biochem. J.* **387,** 67–76
7. Kolodziej, M. P., and Zammit, V. A. (1990) *Biochem. J.* **272,** 421–425
8. Ontko, J. A., and Johns, M. L. (1980) *Biochem. J.* **192,** 959–962
9. Zammit, V. A., Fraser, F., and Orstorphine, C. G. (1997) in *Advances in Enzyme Regulation* (Weber, G., ed) Vol. 37, pp. 295–317, Pergamon Press Ltd., Oxford
10. Mera, P., Bentebibel, A., López-Viñas, E., Cordente, A. G., Gurunathan, C., Sebastián, D., Vázquez, I., Herrero, L., Ariza, X., Gómez-Puertas, P., Asins, G., Serra, D., García, J., and Hegardt, F. G. (2009) *Biochem. Pharmacol.* **77,** 1084–1095
11. Fraser, F., Padovese, R., and Zammit, V. A. (2001) *J. Biol. Chem.* **276,** 20182–20185
12. López-Viñas, E., Bentebibel, A., Gurunathan, C., Morillas, M., de Arriaga, D., Serra, D., Asins, G., Hegardt, F. G., and Gómez-Puertas, P. (2007) *J. Biol. Chem.* **282,** 18212–18224
13. Pan, Y., Cohen, I., Guillerault, F., Fève, B., Girard, J., and Prip-Buus, C. (2002) *J. Biol. Chem.* **277,** 47184–47189
14. Jackson, V. N., Price, N. T., and Zammit, V. A. (2001) *Biochemistry* **40,** 14629–14634
15. Shi, J., Zhu, H., Arvidson, D. N., and Woldegiorgis, G. (1999) *J. Biol. Chem.* **274,** 9421–9426
16. Jackson, V. N., Zammit, V. A., and Price, N. T. (2000) *J. Biol. Chem.* **275,** 38410–38416
17. Jackson, V. N., Cameron, J. M., Zammit, V. A., and Price, N. T. (1999) *Biochem. J.* **341,** 483–489
18. Wu, D., Govindasamy, L., Lian, W., Gu, Y., Kukar, T., Agbandje-McKenna, M., and McKenna, R. (2003) *J. Biol. Chem.* **278,** 13159–13165
19. Cai, Y., Cronin, C. N., Engel, A. G., Ohno, K., Hersh, L. B., and Rodgers, D. W. (2004) *EMBO J.* **23,** 2047–2058
20. Jogl, G., and Tong, L. (2003) *Cell* **112,** 113–122
21. Rufer, A. C., Lomize, A., Benz, J., Chomienne, O., Thoma, R., and Hennig, M. (2007) *FEBS Lett.* **581,** 3247–3252
22. Woldegiorgis, G., Dai, J., and Arvidson, D. (2005) *Mon. Chem.* **136,** 1325–1340
23. Gobin, S., Thuillier, L., Jogl, G., Faye, A., Tong, L., Chi, M., Bonnefont, J. P., Girard, J., and Prip-Buus, C. (2003) *J. Biol. Chem.* **278,** 50428–50434
24. Morillas, M., López-Viñas, E., Valencia, A., Serra, D., Gómez-Puertas, P., Hegardt, F. G., and Asins, G. (2004) *Biochem. J.* **379,** 777–784
25. Kapust, R. B., Tözsér, J., Copeland, T. D., and Waugh, D. S. (2002) *Biochem. Biophys. Res. Commun.* **294,** 949–955
26. Ulmer, T. S., Ramirez, B. E., Delaglio, F., and Bax, A. (2003) *J. Am. Chem. Soc.* **125,** 9179–9191
27. Pervushin, K., Riek, R., Wider, G., and Wüthrich, K. (1997) *Proc. Natl. Acad. Sci. U.S.A.* **94,** 12366–12371
28. Hu, J. S., Grzesiek, S., and Bax, A. (1997) *J. Am. Chem. Soc.* **119,** 1803–1804
29. Kontaxis, G., Clore, G. M., and Bax, A. (2000) *J. Magn. Reson.* **143,** 184–196
30. Jaroniec, C. P., Ulmer, T. S., and Bax, A. (2004) *J. Biomol. NMR* **30,** 181–194
31. Chou, J. J., Delaglio, F., and Bax, A. (2000) *J. Biomol. NMR* **18,** 101–105
32. Grzesiek, S., Anglister, J., and Bax, A. (1993) *J. Magn. Reson. Ser. B* **101,** 114–119
33. Schwieters, C. D., Kuszewski, J. J., Tjandra, N., and Clore, G. M. (2003) *J. Magn. Reson.* **160,** 65–73
34. Shen, Y., Delaglio, F., Cornilescu, G., and Bax, A. (2009) *J. Biomol. NMR* **44,** 213–223
35. Grishaev, A., and Bax, A. (2004) *J. Am. Chem. Soc.* **126,** 7281–7292
36. Kuszewski, J., Gronenborn, A. M., and Clore, G. M. (1997) *J. Magn. Reson.* **125,** 171–177
37. Kiefer, F., Arnold, K., Künzli, M., Bordoli, L., and Schwede, T. (2009) *Nucleic Acids Res.* **37,** D387–D392
38. Shen, Y., Brenke, R., Kozakov, D., Comeau, S. R., Beglov, D., and Vajda, S. (2007) *Proteins* **69,** 734–742
39. Jackson, V. N., Cameron, J. M., Fraser, F., Zammit, V. A., and Price, N. T. (2000) *J. Biol. Chem.* **275,** 19560–19566
40. Jenei, Z. A., Warren, G. Z., Hasan, M., Zammit, V. A., and Dixon, A. M. (2011) *FASEB J.*, in press
41. Kim, H. J., Howell, S. C., Van Horn, W. D., Jeon, Y. H., and Sanders, C. R. (2009) *Prog. Nucl. Magn. Reson. Spectrosc.* **55,** 335–360
42. Warschawski, D. E., Arnold, A. A., Beaugrand, M., Gravel, A., Chartrand, É., and Marcotte, I. (2011) *Biochim. Biophys. Acta* **1808,** 1957–1974
43. Imae, T., and Ikeda, S. (1986) *J. Phys. Chem.* **90,** 5216–5223
44. Bocker, J., Brickmann, J., and Bopp, P. (1994) *J. Phys. Chem.* **98,** 712–717
45. Wishart, D. S., and Case, D. A. (2001) *Methods Enzymol.* **338,** 3–34
46. Spera, S., and Bax, A. (1991) *J. Am. Chem. Soc.* **113,** 5490–5492
47. Gunasekaran, K., Ramakrishnan, C., and Balaram, P. (1997) *Protein Eng.* **10,** 1131–1141
48. Phoenix, D. A., Harris, F., Daman, O. A., and Wallace, J. (2002) *Curr. Protein Pept. Sci.* **3,** 201–221
49. Distler, A. M., Kerner, J., and Hoppel, C. L. (2007) *Biochim. Biophys. Acta* **1774,** 628–636
50. Decatur, S. M. (2000) *Biopolymers* **54,** 180–185
51. Zammit, V. A., Price, N. T., Fraser, F., and Jackson, V. N. (2001) *Biochem. Soc. Trans.* **29,** 287–292
52. Brdiczka, D., Beutner, G., Rück, A., Dolder, M., and Wallimann, T. (1998) *Biofactors* **8,** 235–242
53. Reichert, A. S., and Neupert, W. (2002) *Biochim. Biophys. Acta* **1592,** 41–49
54. Lokappa, S. B., and Ulmer, T. S. (2011) *J. Biol. Chem.* **286,** 21450–21457
55. Bird, M. I., and Saggerson, E. D. (1985) *Biochem. J.* **230,** 161–167
56. Lau, T. L., Kim, C., Ginsberg, M. H., and Ulmer, T. S. (2009) *EMBO J.* **28,** 1351–1361
57. Zammit, V. A. (1983) *Biochem. J.* **214,** 1027–1030
58. Cornell, R. B., and Taneva, S. G. (2006) *Curr. Protein Pept. Sci.* **7,** 539–552
59. Kozlov, M. M., McMahon, H. T., and Chernomordik, L. V. (2010) *Trends Biochem. Sci.* **35,** 699–706
60. Fraser, F., Corstorphine, C. G., and Zammit, V. A. (1997) *Biochem. J.* **323,** 711–718
61. Clamp, M., Cuff, J., Searle, S. M., and Barton, G. J. (2004) *Bioinformatics* **20,** 426–427
62. Baker, N. A., Sept, D., Joseph, S., Holst, M. J., and McCammon, J. A. (2001) *Proc. Natl. Acad. Sci. U.S.A.* **98,** 10037–10041
63. Morillas, M., Gómez-Puertas, P., Bentebibel, A., Sellés, E., Casals, N., Valencia, A., Hegardt, F. G., Asins, G., and Serra, D. (2003) *J. Biol. Chem.* **278,** 9058–9063